Princeton Plasma Physics Laboratory

PPPL-4186

PPPL-4186

On High-frequency Gyrokinetics in Magnetically-confined Plasmas

R.A. Kolesnikov, W.W. Lee, H. Qin, and E. Startsev

October 2006

Prepared for the U.S. Department of Energy under Contract DE-AC02-76CH03073.

Princeton Plasma Physics Laboratory
Report Disclaimers

Full Legal Disclaimer

Trademark Disclaimer

PPPL Report Availability

Princeton Plasma Physics Laboratory

This report is posted on the U.S. Department of Energy's Princeton Plasma Physics Laboratory Publications and Reports web site in Fiscal Year 2006.

The home page for PPPL Reports and Publications is:

http://www.pppl.gov/pub_report/

Office of Scientific and Technical Information (OSTI):

Available electronically at: http://www.osti.gov/bridge.

Available for a processing fee to U.S. Department of Energy and its contractors, in paper from:

U.S. Department of Energy
Office of Scientific and Technical Information
P.O. Box 62
Oak Ridge, TN 37831-0062

Telephone: (865) 576-8401

Fax: (865) 576-5728

E-mail: reports@adonis.osti.gov

On High-Frequency Gyrokinetics in Magnetically-Confined Plasmas

R. A. Kolesnikov, W. W. Lee, H. Qin and E. Startsev
Plasma Physics Laboratory, Princeton University, P.O. Box 451, Princeton, New Jersey 08543
(Dated: September 25, 2006)

The physics of high-frequency gyrokinetics in magnetized plasmas is explored, based on the gyrocenter-gauge kinetic theory in the limit of gyroradius much smaller than the scale length of the magnetic field. Contrary to low-frequency gyrokinetics, which views each particle as a rigid charged ring, we found that, from the arbitrary frequency point of view, a particle can be described by a rubber-band-like structure. A computational algorithm based on this concept has been developed and its application to the current-driven electrostatic ion cyclotron instability is presented.

PACS numbers: 52.30.Gz, 52.50.Qt, 52.35.Hr

The importance of gyrokinetic theory [1–4] for plasmas in a strong magnetic field has been widely appreciated. By removing the high frequency dynamics associated with fast gyromotion from the original kinetic system, the gyrokinetic formalism yields a system of equations for description of low frequency ($\omega \ll \Omega$, where Ω is the cyclotron frequency) and long wavelength phenomena in plasmas. However, the physics associated with the omitted high frequency part may be important. Particularly, in fusion plasmas, electromagnetic waves in the radio frequency (rf) range are used for plasma heating in resonant layers. Some of the approaches utilized for studying the interaction between rf waves and plasmas include Fokker-Plank Solvers [5] and Monte Carlo simulation [6]. In this paper we present an alternative computational algorithm, which allows one to study the high frequency part of the dynamics within the gyrokinetic framework. One of the immediate advantages of an algorithm based on the gyrokinetic formulation is that it may be suitable for implementation into existing sophisticated gyrokinetic codes [7] developed to study low frequency turbulence phenomena in general geometry. Contrary to low frequency gyrokinetics, which views each particle as a rigid charged ring, we will show that, if arbitrary frequency dynamics is being studied, a gyrokinetic particle needs to be described by a special rubber-band-like structure.

The high frequency gyrokinetic model we discuss in this paper is based on the gyrocenter-gauge kinetic theory, developed by Qin *et al.* [8, 9] in the limit of particle gyroradius much smaller than the scale length of the ambient magnetic field, $\rho/L_B \ll 1$. The gyrokinetic formalism performs the transformation from the particle coordinate system $(\boldsymbol{x}, \boldsymbol{v})$ to a new gyrocenter coordinate system $\overline{\boldsymbol{Z}} = (\overline{\boldsymbol{X}}, \overline{U}, \overline{\mu}, \overline{\xi})$. Here, $\overline{\boldsymbol{X}}$ and $\overline{U}$ are the location and parallel velocity of the particle gyrocenter, $\overline{\mu}$ is the magnetic moment and $\overline{\xi}$ is the gyrophase angle. $f(\overline{\boldsymbol{Z}}, t)$ is the distribution function in the new coordinates, where the parallel (gyrocenter) and the perpendicular (gyrophase) dynamics are decoupled.

The parallel dynamics is given by the evolution of the gyrophase-averaged part of the distribution function $F(\overline{\boldsymbol{Z}}, t) \doteq \langle f(\overline{\boldsymbol{Z}}, t) \rangle$ according to

$$\frac{\partial F}{\partial t} + \dot{\overline{\boldsymbol{X}}} \cdot \frac{\partial F}{\partial \overline{\boldsymbol{X}}} + \dot{\overline{U}} \frac{\partial F}{\partial \overline{U}} = 0. \tag{1}$$

Here, the notation for a gyrophase-averaged quantity is introduced by $\langle a \rangle \doteq (2\pi)^{-1} \int a d\overline{\xi}$.

For a simple electrostatic system with no magnetic field inhomogeneities, the perpendicular gyrophase dependent part of the dynamics (for $e\Phi/T \ll 1$) is described by the generating (gauge) function $S(\overline{\boldsymbol{Z}}, t)$ according to [8]

$$\frac{\partial S}{\partial t} + \Omega \frac{\partial S}{\partial \overline{\xi}} + \dot{\overline{\boldsymbol{X}}} \cdot \frac{\partial S}{\partial \overline{\boldsymbol{X}}} + \dot{\overline{U}} \frac{\partial S}{\partial \overline{U}} = q \widetilde{\Phi}(\overline{\boldsymbol{X}} + \boldsymbol{\rho}, t), \tag{2}$$

where the following notation is introduced $\widetilde{a} \doteq a - \langle a \rangle$.

An appropriate adiabatic invariant $\overline{\mu}$ is obtained by expansion up to the first order term in the smallness parameter $\rho/L_B \ll 1$, and is given by

$$\overline{\mu} = \mu + \widehat{\boldsymbol{Q}}_\xi S, \quad \widehat{\boldsymbol{Q}}_\xi \doteq \frac{q}{mc} \frac{\partial}{\partial \overline{\xi}}. \tag{3}$$

where $\mu = m v_\perp^2 / 2B$. The quantity $\overline{\mu}$ is an approximation to the true magnetic moment, which is conserved. The quantities m and q stand for the particle mass and charge.

Self-consistency is obtained by solving the Poisson equation (s denotes species)

$$\nabla^2 \Phi(\boldsymbol{x}, t) = -4\pi \sum_s q_s \int f_s(\boldsymbol{x}, \boldsymbol{v}, t) d\boldsymbol{v}, \tag{4}$$

where $f(\boldsymbol{x}, \boldsymbol{v}, t)$ is the distribution function in particle coordinates. The density on the right hand side is

$$\begin{aligned} \int f_s(\boldsymbol{x}, \boldsymbol{v}, t) d\boldsymbol{v} &= \int f_s(\overline{\boldsymbol{Z}}, t) \delta(\overline{\boldsymbol{X}} - \boldsymbol{x} + \boldsymbol{\rho}) d\overline{\boldsymbol{Z}} \\ &= \int (1 + \delta \mathsf{T}) F_s(\overline{\boldsymbol{Z}}, t) \delta(\overline{\boldsymbol{X}} - \boldsymbol{x} + \boldsymbol{\rho}) d\overline{\boldsymbol{Z}}. \end{aligned} \tag{5}$$

In the gyrocenter coordinates a near-identity transformation $\mathsf{T} = 1 + \delta \mathsf{T}$ divides the particle density into two parts. The first part is due to the gyrocenter distribution function $F(\overline{\boldsymbol{Z}}, t)$. The second part is the contribution due

to the gyrophase dependent part of the distribution function $\delta\mathsf{T}F(\overline{\boldsymbol{Z}},t) = F(\overline{\boldsymbol{Z}},t)\widehat{\boldsymbol{Q}}_{\mathsf{T}}S(\overline{\boldsymbol{Z}},t)$ with

$$\widehat{\boldsymbol{Q}}_{\mathsf{T}} \doteq \frac{q}{mc}\frac{\partial \ln F}{\partial \overline{\mu}}\frac{\partial}{\partial \overline{\xi}} + \frac{1}{m}\frac{\partial \ln F}{\partial \overline{U}}\widehat{\boldsymbol{b}}\cdot\frac{\partial}{\partial \overline{\boldsymbol{X}}} - \frac{1}{\Omega m}\frac{\partial \ln F}{\partial \overline{\boldsymbol{X}}}\cdot\widehat{\boldsymbol{b}}\times\frac{\partial}{\partial \overline{\boldsymbol{X}}}, \tag{6}$$

which describes polarization effects due to gyromotion. The unit vector $\widehat{\boldsymbol{b}}$ is along the ambient magnetic field.

Low frequency gyrokinetics only solves Eq. (1) along with an appropriate gyrokinetic Poisson equation [3]. The motion of a particle may be imagined as the motion of its gyrocenter with a constant uniformly charged ring attached to it (Fig. 1). The purpose of this ring is to take FLR effects into account by appropriate averaging technique via a finite number of points on each ring [10].

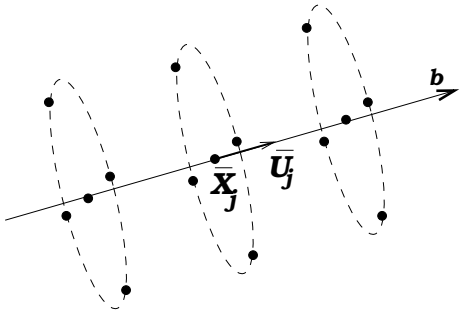

FIG. 1: Motion of a particle from the low frequency gyrokinetic point of view. Particle j has gyrocenter located at $\overline{\boldsymbol{X}}_j$ with parallel velocity $\overline{U}_j$. Each gyrocenter has a constant charged ring attached to it. An appropriate gyro-averaging is performed on a finite number of points on each ring.

In the arbitrary frequency regime, Eqs. (1) and (2) for the gyrocenter and gyrophase dynamics need to be solved together with the Poisson Eq. (4) and the constraint on the magnetic moment Eq. (3). This system constitutes our model for slab geometry in the electrostatic limit. The gyrocenter dynamics described by Eq. (1) is easily simulated by a *gyrocenter pusher* [10], which advances each particle's gyrocenter location and parallel velocity. Particularly, for particle j we have

$$\dot{\overline{\boldsymbol{X}}}_j = \overline{U}_j\widehat{\boldsymbol{b}} + \frac{q}{\Omega m}\langle \boldsymbol{E}_j\rangle\times\widehat{\boldsymbol{b}}, \tag{7}$$

$$\dot{\overline{U}}_j = \frac{q}{m}\langle \boldsymbol{E}_j\rangle\cdot\widehat{\boldsymbol{b}}. \tag{8}$$

where $\langle \boldsymbol{E}_j\rangle$ is gyrophase-averaged electric field at the particle location. If δf-simulation [11] is used, then each particle will also have a gyrocenter weight w_j associated with it. Particularly, if $F = F_0 + \delta f$, then $w_j = \delta f/F|_j$ and

$$\dot{w}_j = -(1-w_j)\Big(\frac{q}{m}\langle \boldsymbol{E}_j\rangle\cdot\widehat{\boldsymbol{b}}\frac{\partial}{\partial \overline{U}_j} + \frac{q}{\Omega m}\langle \boldsymbol{E}_j\rangle\times\widehat{\boldsymbol{b}}\cdot\frac{\partial}{\partial \overline{\boldsymbol{X}}_j}\Big)\ln F_0 \tag{9}$$

The gyrophase dependent part of the dynamics described by the equation for the generating function Eq. (2) may be simulated by a *gyrophase pusher*, which solves for functions $g_{\mathsf{T}}(\overline{\boldsymbol{Z}},t)$ and $g_\xi(\overline{\boldsymbol{Z}},t)$, where

$$g_{\mathsf{T}} \doteq \widehat{\boldsymbol{Q}}_{\mathsf{T}}S, \quad g_\xi \doteq \widehat{\boldsymbol{Q}}_\xi S. \tag{10}$$

The dynamical equations for these quantities are

$$\Big(\frac{\partial}{\partial t} + \Omega\frac{\partial}{\partial \overline{\xi}} + \dot{\overline{\boldsymbol{X}}}\cdot\frac{\partial}{\partial \overline{\boldsymbol{X}}} + \dot{\overline{U}}\frac{\partial}{\partial \overline{U}}\Big)g_{\mathsf{T}} = q\widehat{\boldsymbol{Q}}_{\mathsf{T}}\widetilde{\Phi}(\overline{\boldsymbol{X}}+\boldsymbol{\rho},t),$$

$$\Big(\frac{\partial}{\partial t} + \Omega\frac{\partial}{\partial \overline{\xi}} + \dot{\overline{\boldsymbol{X}}}\cdot\frac{\partial}{\partial \overline{\boldsymbol{X}}} + \dot{\overline{U}}\frac{\partial}{\partial \overline{U}}\Big)g_\xi = q\widehat{\boldsymbol{Q}}_\xi\widetilde{\Phi}(\overline{\boldsymbol{X}}+\boldsymbol{\rho},t).$$

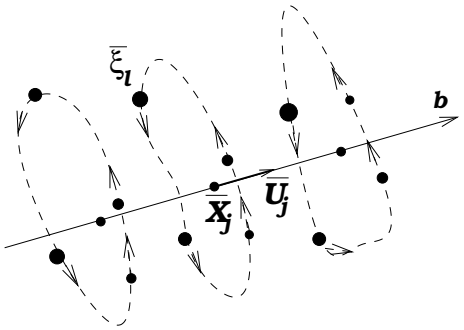

FIG. 2: Motion of a particle from the arbitrary frequency gyrokinetic point of view. Particle j has its gyrocenter located at $\overline{\boldsymbol{X}}_j$ with parallel velocity $\overline{U}_j$. Each gyrocenter has a rubber band structure attached to it, which is changing with time in a plane perpendicular to the magnetic field. An appropriate gyrophase-averaging is performed on a finite number of points ($p = 4$ in this figure) with different $\overline{\xi}_l$ on each rubber band. These points have different sizes to represent the amount of gyrophase weight attached to them.

In the arbitrary frequency case, the motion of a particle from the gyrokinetic point of view is more complicated than in the low frequency regime. As time goes on, each particle j's gyrocenter is moving according to Eqs. (7)–(9). Also each gyrocenter has a *rubber band* kind of entity attached to it, whose form (the dependence of gyroradius versus gyrophase) is determined by the rotation with the cyclotron frequency $\dot{\overline{\xi}} = \Omega$, together with conservation of the magnetic moment Eq. (3), which takes the following form

$$\overline{\mu}_j(\overline{\xi}) = \frac{q}{mc}\frac{v_{\perp j}^2(\overline{\xi},t)}{2\Omega} + g_\xi(\overline{\boldsymbol{Z}}_j,t), \tag{11}$$

$$\dot{g}_\xi(\overline{\boldsymbol{Z}}_j,t) = -\frac{q^2}{\Omega mc}\widetilde{\boldsymbol{E}}_j\cdot\boldsymbol{v}_{\perp j}. \tag{12}$$

This rubber band structure is quickly changing with time in a plane perpendicular to the magnetic field and is different for each particle. Each of these rubber bands has a *gyrophase weight function* $g_{\mathsf{T}}(\overline{\boldsymbol{Z}}_j,t)$, which is evolving

according to

$$\dot{g}_{\mathsf{T}}(\overline{\boldsymbol{Z}}_j,t) = -\Big(\frac{q^2}{\Omega mc}\widetilde{\boldsymbol{E}}_j\cdot\boldsymbol{v}_{\perp j}\frac{\partial}{\partial\overline{\mu}_j}+\frac{q}{m}\widetilde{\boldsymbol{E}}_j\cdot\widehat{\boldsymbol{b}}\frac{\partial}{\partial\overline{U}_j} + \frac{q}{\Omega m}\widetilde{\boldsymbol{E}}_j\times\widehat{\boldsymbol{b}}\cdot\frac{\partial}{\partial\overline{\boldsymbol{X}}_j}\Big)\ln F_0. \quad (13)$$

In real simulations, only a finite number of points on each rubber band are followed (Fig. 2). For a particular particle j, we use index l to enumerate simulation points (with the same $\overline{\boldsymbol{X}}_j$ and $\overline{U}_j$, but different $\overline{\xi}_l$'s) on its rubber band. Then the dynamics of point l are determined by $\overline{\mu}_j(\overline{\xi}_l)=$ const and quantity $g_{\mathsf{T}}(\overline{\boldsymbol{Z}}_j(\overline{\xi}_l),t)$.

The simulation is done self-consistently by calculating the Poisson equation

$$\nabla^2\Phi(\boldsymbol{x},t) = -4\pi\sum_s q_s\sum_j\frac{2\pi}{p}\sum_{l=1}^{p} \quad (14)$$
$$\times\Big(w_j(t)+g_{\mathsf{T}}(\overline{\boldsymbol{Z}}_j(\overline{\xi}_l),t)\Big)\delta\left(\overline{\boldsymbol{X}}_j(t)-\boldsymbol{x}+\boldsymbol{\rho}_j(\overline{\xi}_l,t)\right),$$

where on the right hand side the first term is the perturbed gyrocenter density, while the second term is due to the gyrophase part of the dynamics. The last sum represents the summation over p points on each rubber band to approximate an appropriate gyrophase integration. The accuracy of this approximation is determined by the resolution of the gyrophase subspace by the total number of points on all rubber bands [12]. In conventional low frequency gyrokinetics, the evolution of the rubber bands together with the gyrophase weight function is not present explicitly, but instead is contained in the polarization density term on the left hand side of the gyrokinetic Poisson equation [3].

Our ultimate interest is to study the interactions of rf waves with magnetized plasmas in realistic situations. Our model can easily be generalized to describe electromagnetic systems and arbitrary geometry configurations [8]. In the limit of small gyroradius $\rho/L_B \ll 1$, this approach is equivalent to integration of the Lorentz force equations along particle orbits. But as opposed to the latter approach, the present algorithm is suitable for implementation into existing low frequency gyrokinetic codes. Also, separation of motions gives one more flexibility for algorithm manipulation and optimization, which will be discussed in future publications [12].

For the simple electrostatic case we study in this paper, the only new physics introduced by the high frequency gyrophase dependent part of the dynamics is cyclotron waves. In this paper we apply the algorithm described above only to ions, with electrons being treated drift-kinetically. We use the example of the ion cyclotron instability [13] to illustrate mechanisms introduced by high frequency gyrophase dynamics into the gyrokinetic formalism. In this case the electrons have a shifted Maxwellian distribution with parallel drift $v_{de}\neq 0$. Some of the cyclotron harmonics are subject to inverse electron Landau damping. We performed two-dimensional simulation of the cyclotron instability with the HFGK code for $\omega_{pi}/\Omega_i = 10.0$, $k_{||}=0.1k_\perp$, $v_{de}=v_{te}$ and equal electron and ion temperatures. The system has a 16×16 grid with one ion gyroradius being the size of two grid cells. Fig. 3 shows the time dependence of the $k_\perp\rho_i=0.8$ mode from the HFGK code with $4\cdot10^5$ gyrocenters (and $p=1$).

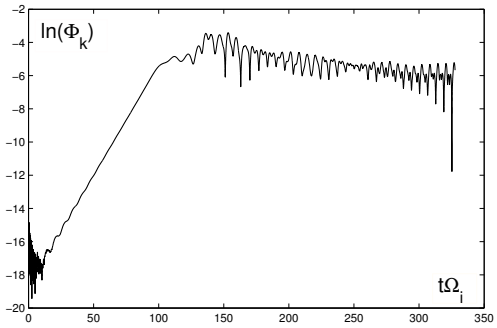

FIG. 3: Dependence of $\ln\Phi_k$ vs. $t\Omega_i$ for the $k_\perp\rho_i=0.8$ mode from the HFGK code with $4\cdot10^5$ gyrocenters. Each particle's rubber band is approximated by one point, $p=1$.

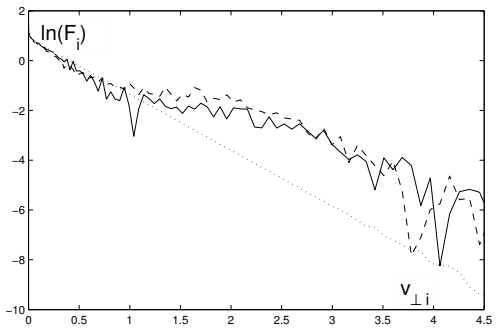

FIG. 4: Ion perpendicular distribution function (on a logarithmic scale) at $t\Omega_i\approx330$. The dotted line is the initial Maxwellian distribution function. The solid line is from the HFGK code, while the dashed line is from a Lorentz-force code.

The code gives a linear growth rate for the cyclotron instability which is consistent with analytical predictions from an appropriate dispersion relation [13]. The first harmonic of the $k_\perp\rho_i=0.8$ mode is the most unstable one in the linear regime. While it saturates at $t\Omega_i\approx80$, the second harmonic continues to grow until $t\Omega_i\approx140$ and thus prevails in the nonlinear regime. The saturation of the cyclotron instability is due to quasilinear flattening of the electron parallel velocity distribution, which quenches the free energy for the instability.

Fig. 4 shows the ion perpendicular distribution functions (on a logarithmic scale) at the end of the simulations corresponding to the HFGK code (solid line) and a

Lorentz-force code (dashed line) with $4 \cdot 10^5$ particles. The initial Maxwellian distribution function is given by the dotted line. Both codes show the development of a non-Maxwellian tail, which indicates that the energy is deposited into ion perpendicular motion. This is a nonlinear heating mechanism due to a random walk process in velocity space a gyrating particle goes through in the presence of many randomly phased waves in the system. In our algorithm the dynamics of perpendicular heating is mostly described by evolution of the rubber band structures [12]. On average, the ions are heated by the electric field. In these simple simulations, we do not have density and magnetic field inhomogeneities, which produce uniform in space ion perpendicular heating. In realistic simulations, the heating would occur mostly in cyclotron resonance layers.

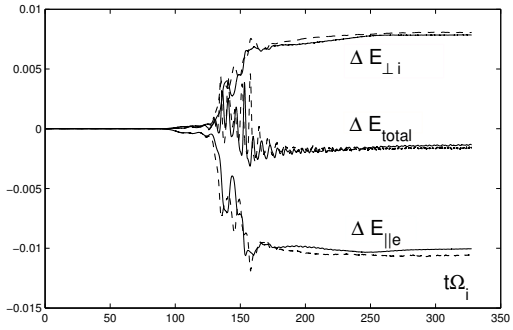

FIG. 5: Time dependence of changes in ion perpendicular kinetic energy $\mathcal{E}_{\perp i}$, electron parallel kinetic energy $\mathcal{E}_{||e}$ and total energy $\mathcal{E}_{total}$. These quantities are normalized to the ion temperature. Solid lines are from the HFGK code, while dashed lines are from the Lorentz-force code.

Fig. 5 shows the time dependences of changes in ion perpendicular kinetic energy $\mathcal{E}_{\perp i}$, electron parallel kinetic energy $\mathcal{E}_{||e}$ and total energy $\mathcal{E}_{total}$. The total energy includes electron parallel kinetic energy, both ion parallel and perpendicular kinetic energy, and electrostatic energy contributions. In the HFGK code, the quantities $\mathcal{E}_{||s}$ and $\mathcal{E}_{\perp i}$ are found from

$$\mathcal{E}_{||s}(t) = \frac{m_s}{2} \sum_j \overline{U}_j^2(t), \tag{15}$$

$$\mathcal{E}_{\perp i}(t) = \frac{m_i}{2} \sum_j \sum_l v_{\perp j}^2(\overline{\xi}_l, t). \tag{16}$$

The solid lines are from the HFGK code, while the dashed lines are from the Lorentz-force code. The total energy $\mathcal{E}_{total}$ is not precisely conserved in both codes, because the δf calculation needs a sufficiently large number of particles and modes to be able to more accurately describe quasilinear flattening of the electron parallel distribution function. Since an arbitrary number of points on each rubber band may be used, the HFGK simulation is more flexible from the phase space resolution point of view than the more straightforward Lorentz force approach. Further results will be reported elsewhere [12].

The nonlinear ion perpendicular heating we observed is described in the present algorithm via first principles based physics of the interaction between the cyclotron waves and the particle's gyrophase dynamics. Like the Lorentz-force approach, our algorithm does not make assumptions about the quasilinear nature of the dynamics and does not need to introduce an rf-induced random walk model to describe the diffusion in velocity space.

In summary, a high frequency gyrokinetic particle-in-cell algorithm was developed, which allows one to simulate arbitrary frequency and wavelength physics for $\rho/L_B \ll 1$ and $e\Phi/T \ll 1$. This approach is based on the gyrocenter-gauge kinetic theory, which transforms the original Vlasov equation to a system of decoupled equations for the gyrocenter and gyrophase dynamics. We found that arbitrary frequency gyrokinetics describes each particle as a complicated, quickly changing rubber-band-like structure. The algorithm allows a self-consistent simulation of the interaction between rf waves and plasma, based on first principle physics. The approach is suitable for implementation into global gyrokinetic codes to study the nonlinear rf heating dynamics resulting in non-Maxwellian tails in distribution functions. This approach also allows us to study the effects that turbulence, driven by low frequency drift-like microinstabilities, may have on the heating dynamics.

The present work was supported by the Multi-Scale Gyrokinetics (MSG) project as a part of the U. S. DoE ASCR Multiscale Mathematics Research and Education Program.

[1] R. G. Littlejohn, Phys. Fluids **24**, 1730 (1981).
[2] A. J. Brizard, J. Plasma Phys. **41**, 541 (1989).
[3] W. W. Lee, Phys. Fluids **26**, 556 (1983).
[4] D. H. E. Dubin, J. A. Krommes, C. Oberman and W. W. Lee, Phys. Fluids **26**, 3524 (1983).
[5] E. F. Jaeger, L. A. Berry, S. D. Ahern, R. F. Barrett *et al.*, Phys. Plasmas **13**, 6101 (2006).
[6] M. Choi, V. S. Chan, R. I. Pinsker, S. C. Chiu and W. W. Heidbrink, Phys. Plasmas **12**, 2505 (2005).
[7] Z. Lin, T. S. Hahm, W. W. Lee, W. M. Tang and R. B. White, Science **281**, 1835 (1998).
[8] H. Qin, W. M. Tang, W. W. Lee and G. Rewoldt, Phys. Plasmas **6**, 1575 (1999).
[9] H. Qin, W. M. Tang and W. W. Lee, Phys. Plasmas **7**, 4433 (2000).
[10] W. W. Lee, J. Comput. Phys. **72**, 243 (1987).
[11] S. E. Parker and W. W. Lee, Phys. Fluids B **5**, 77 (1993).
[12] R. Kolesnikov, W. W. Lee, H. Qin and E. Startsev, in preparation.
[13] H. Okuda, C. Z. Cheng and W. W. Lee, Phys. Fluids **24**, 1060 (1981).

The Princeton Plasma Physics Laboratory is operated
by Princeton University under contract
with the U.S. Department of Energy.

Information Services
Princeton Plasma Physics Laboratory
P.O. Box 451
Princeton, NJ 08543

Phone: 609-243-2750
Fax: 609-243-2751
e-mail: pppl_info@pppl.gov
Internet Address: http://www.pppl.gov